

Multi-species laser absorption sensors for in situ monitoring of syngas composition

Ritobrata Sur · Kai Sun · Jay B. Jeffries ·
Ronald K. Hanson

Received: 28 January 2013 / Accepted: 28 June 2013 / Published online: 14 July 2013
© Springer-Verlag Berlin Heidelberg 2013

Abstract Tunable diode laser absorption spectroscopy sensors for detection of CO, CO₂, CH₄ and H₂O at elevated pressures in mixtures of synthesis gas (syngas: products of coal and/or biomass gasification) were developed and tested. Wavelength modulation spectroscopy (WMS) with 1f-normalized 2f detection was employed. Fiber-coupled DFB diode lasers operating at 2325, 2017, 2290 and 1352 nm were used for simultaneously measuring CO, CO₂, CH₄ and H₂O, respectively. Criteria for the selection of transitions were developed, and transitions were selected to optimize the signal and minimize interference from other species. For quantitative WMS measurements, the collision-broadening coefficients of the selected transitions were determined for collisions with possible syngas components, namely CO, CO₂, CH₄, H₂O, N₂ and H₂. Sample measurements were performed for each species in gas cells at a temperature of 25 °C up to pressures of 20 atm. To validate the sensor performance, the composition of synthetic syngas was determined by the absorption sensor and compared with the known values. A method of estimating the lower heating value and Wobbe index of the syngas mixture from these measurements was also demonstrated.

1 Introduction

Coal represents the most widely used hydrocarbon fuel for generation of electricity in the world. However, there is growing concern about the release of greenhouse and

poisonous gases such as CO₂, SO₂, H₂S and NO_x as a result of the combustion of coal. Integrated gasification-combined cycle (IGCC) power generation is one of the cleanest methods of extracting energy from coal [1, 2] with highly efficient CO₂ and sulfur sequestration processes. One of the main components of the IGCC system is the coal gasifier, which converts coal into synthesis gas (syngas) comprised mainly of CO, CO₂ and H₂. The CO₂ typically is removed from this mixture, and the remainder is fed into the gas turbine along with air and/or oxygen. Such systems require monitoring of the syngas composition to indicate the extent of reaction in the gasifier and the heating value of the output synthesis gas or syngas. Conventionally, an extractive method can be used to analyze the components of the syngas with industrially available sensors. However, often the sample extraction and preparation (depressurization, cooling, dehumidification and filtration of particulates) significantly delay the time response, and a faster control variable is required. Solution of this syngas analysis problem has been recognized as a crucial requirement for the improvement of control and instrumentation of gasifiers by the US Department of Energy [3]. Reported here is the development of a robust high-pressure gas sensor for the in situ detection of the syngas components in harsh particulate-laden environments based on laser absorption.

Tunable diode lasers (TDLs) offer high promise for providing a sensor with the desired characteristics. The advantages of the TDL-based sensors are fast response, non-intrusive nature and sensitive species-specific detection capabilities. TDL sensors have been demonstrated previously to monitor the gases in different combustion systems [4–9], for environmental monitoring [10–12] and other energy conversion devices [13]. Our initial work in coal gasifiers to monitor the temperature and water concentration has been discussed by Sun et al. [14]. Here, we

R. Sur (✉) · K. Sun · J. B. Jeffries · R. K. Hanson
High Temperature Gas dynamics Laboratory, Department of
Mechanical Engineering, Stanford University, Stanford, CA
94305, USA
e-mail: rsur@stanford.edu

present the design rules and validation testing of the gas composition sensors mentioned in that work. Other related literature includes the detection of HCl in atmospheric pressure syngas [15].

Some of the problems of developing an optical sensor unique to the gasification environments are the following:

1. A particulate-laden environment with extremely low transmission [16].
2. The high pressure of efficient gasification processes [2] produces collision broadening of the absorption transition leading to a decreased peak signal and an absence of the non-absorbing baseline typically used with direct-absorption spectroscopy.

These problems were overcome by the use of a 1f-normalized WMS-2f technique that has been demonstrated previously to be effective in high pressure and noisy environments [17, 18]. In this method, the injection laser current of the diode laser is modulated sinusoidally producing a simultaneous variation in laser output intensity and frequency. The signal transmitted through the absorption medium is analyzed at the integer multiples of the modulation frequency; hence, the terminology 1f, 2f, and so on. This technique is well-known for noise rejection in the detection of trace species [5–7, 9–12] and has been used at Stanford University in noisy environments [4, 8, 18]. This normalization technique accounts for the variations in non-absorption losses of the transmitted laser intensity [17–19].

The current sensor uses four lasers for detection of CO, CO₂, CH₄ and H₂O at the center frequencies of 4,301, 4,957, 4,367 (Nanoplus), and 7,394 (NEL) cm⁻¹ (2,325, 2,017, 2,290, and 1,352 nm). The remainder of the gas is assumed to be H₂, thus accounting for the major species in the syngas. With this information, the heating value and the Wobbe index of the syngas can be monitored as a part of a real-time control loop. This article describes the sensor design and validates performance in a laboratory environment with known gas composition.

2 Theory

A great deal of work has been done in the past [17, 18, 20–23] to develop an accurate WMS model for large modulation depths needed for absorption sensing at elevated pressure. A summary is presented here to guide the reader and define the notation.

The laser is modulated by sinusoidally varying injection current at angular frequency $\omega = 2\pi f$ which results in an intensity and frequency response as follows:

$$I_0(t) = \bar{I}_0[1 + i_1 \cos(\omega t + \psi_1) + i_2 \cos(2\omega t + \psi_2)] \quad (1)$$

$$\nu(t) = \bar{\nu} + a \cos(\omega t + \psi) \quad (2)$$

where ν is the frequency of light at time t , $\bar{\nu}$ is the center frequency, a is the modulation depth, ψ is the initial phase of the frequency modulation, I_0 is the unabsorbed beam intensity, \bar{I}_0 is the average intensity at the center frequency, i_1 is the linear (1f) intensity modulation amplitude, i_2 is the second-order (2f) intensity modulation amplitude, and ψ_1 and ψ_2 are the initial phases of the first- and second-order intensity modulation. For the lasers used currently, the higher-order intensity modulation terms were found to be negligible. But if faced with a highly nonlinear DFB diode laser performance, such effects could be taken into account as shown by Sun et al. [23].

From the Beer–Lambert law, it is known that the transmission coefficient (τ) of a monochromatic light beam at frequency ν is governed by the relation:

$$\tau(\nu) = \frac{I}{I_0} = e^{-\alpha(\nu)} \quad (3)$$

where I_0 is the incident beam intensity, I is the transmitted beam intensity and α is the spectral absorbance for a pressure P , path length L , mole fraction of the i th absorbing species x_i , transition line strength $S_{i,j}$ and lineshape function $\phi_{i,j}(\nu)$ of the j th transition, as defined by the expression

$$\alpha(\nu) = P \cdot L \cdot \sum_{i,j} x_i \cdot S_{i,j} \cdot \phi_{i,j}(\nu) \quad (4)$$

The above expression assumes uniform gas composition and temperature along the laser line of sight (LOS). For an isolated transition, the total area under the absorbance curve is given by:

$$\int_{-\infty}^{\infty} \alpha(\nu) d\nu = P \cdot x_i \cdot L \cdot S_{i,j} \quad (5)$$

The lineshape function $\phi_{i,j}(\nu)$ is approximated by a Voigt function characterized by the collision-broadened full-width at half-maximum (FWHM), $\Delta\nu_{c,i}$ [cm⁻¹] and the Doppler FWHM, $\Delta\nu_d$ [cm⁻¹]. The collisional FWHM is given by the expression:

$$\Delta\nu_{c,i} = P \sum_j x_j 2\gamma_{ij} \quad (6)$$

The dependence of the collision-broadening factor on temperature can be modeled as a power law expression:

$$\gamma_{ij}(T) = \gamma_{ij}(T_{\text{ref}}) \cdot \left(\frac{T_{\text{ref}}}{T}\right)^{n_j} \quad (7)$$

where T_{ref} is the reference temperature (chosen to be 296 K) and n_j is the temperature-dependence index.

Due to the sinusoidal modulation at a frequency ω of the laser wavelength, the resulting transmission is also periodic

with a period ω . Therefore, it can be expressed as a Fourier series expansion as follows:

$$\tau(t) = \sum_{k=0}^{\infty} H_k \cos(k\omega t) \tag{8}$$

where H_k is the k th Fourier coefficient of the expansion and can be expressed as:

$$H_k = \frac{1}{(1 + \delta_{k0})\pi} \int_{-\pi}^{\pi} \tau(\bar{\nu} + a \cos \theta) \cdot \cos(k\theta) d\theta \tag{9}$$

By combining Eqs. (2), (3) and (8), we get the transmitted laser intensity:

$$I(t) = \bar{I}_0 [1 + i_1 \cos(\omega t + \psi_1) + i_2 \cos(2\omega t + \psi_2)] \left[\sum_{k=0}^{\infty} H_k \cos(k\omega t) \right] \tag{10}$$

No assumptions were made about the optical depth in this expression, and thus, it can be used with any level of absorbance. A crucial part of the WMS technique involves extraction of the harmonics of the above signal at integral multiples of the modulation frequency ω . This is achieved using a digital lock-in amplifier, where the above signal obtained from the detector is first multiplied by $\cos(n\omega t)$ or $\sin(n\omega t)$, after which a low-pass filter for the X and Y components, respectively, can yield the nf signal. The resulting equations for the X and Y components of the 1f and 2f signals are given by (as previously shown by Rieker et al. [18]):

$$X_{1f} = \frac{G\bar{I}_0}{2} \times \left[H_1 + i_1 \left\{ H_0 + \frac{H_2}{2} \right\} \cos(\psi_1 - \psi) + \frac{i_2}{2} \{ H_1 + H_3 \} \cos(\psi_2 - \psi) \right] \tag{11}$$

$$Y_{1f} = \frac{G\bar{I}_0}{2} \times \left[i_1 \left\{ \frac{H_2}{2} - H_0 \right\} \sin(\psi_1 - \psi) + \frac{i_2}{2} \{ H_3 - H_1 \} \sin(\psi_2 - \psi) \right] \tag{12}$$

$$X_{2f} = \frac{G\bar{I}_0}{2} \times \left[\underbrace{\frac{i_1}{2} \{ H_1 + H_3 \} \cos(\psi_1 - \psi)}_{\text{Asymmetric}} + \underbrace{\frac{i_2}{2} \left\{ \frac{H_4}{2} + H_0 \right\} \cos(\psi_2 - \psi) + H_2}_{\text{Symmetric}} \right] \tag{13}$$

$$Y_{2f} = \frac{G\bar{I}_0}{2} \times \left[\underbrace{\frac{i_1}{2} \{ H_3 - H_1 \} \sin(\psi_1 - \psi)}_{\text{Asymmetric}} + \underbrace{\frac{i_2}{2} \left\{ \frac{H_4}{2} + H_0 \right\} \sin(\psi_2 - \psi)}_{\text{Symmetric}} \right] \tag{14}$$

where G is the overall electro-optic gain in the signal that includes the attenuation due to beam blockage by particles. The 1f signal magnitude is given by

$$R_{1f} = \sqrt{X_{1f}^2 + Y_{1f}^2} \tag{15}$$

The 2f by 1f normalization scheme with background subtraction used in this work is identical to the one used by Rieker et al. [18]:

$$S_{2f/1f} = \sqrt{\left[\left(\frac{X_{2f}}{R_{1f}} \right)_{\text{raw}} - \left(\frac{X_{2f}}{R_{1f}} \right)_{\text{bg}} \right]^2 + \left[\left(\frac{Y_{2f}}{R_{1f}} \right)_{\text{raw}} - \left(\frac{Y_{2f}}{R_{1f}} \right)_{\text{bg}} \right]^2} \tag{16}$$

This normalization scheme cancels the factor G that accounts for the majority of random fluctuations in the average signal due to laser noise and non-absorption transmission losses, resulting in a robust sensor applicable in harsh environments.

3 Effects of collision broadening on modulation optimization

The WMS signal depends on the absorbance, the lineshape and the range of the wavelength modulation. Thus, optimization of the modulation parameters must include consideration of collision broadening. First, we consider an absorber with a single isolated transition. This fictitious species is approximated by the P24 transition of the 20012 \leftarrow 00001 band of CO₂ near 4,957 cm⁻¹. Simulating a scanned-WMS lineshape requires the parameters for both the transition and the TDL wavelength modulation as given in Table 1.

The wavelength-scanned direct-absorption simulation of the single isolated transition is shown in Fig. 1a for 10 % absorber in air at 5 and 12 atm. All the simulations were done using the Humlicek [24] Voigt lineshape model. For pressures above 0.5 atm, collision broadening dominates over Doppler broadening resulting in a predominantly

Table 1 Parameters for simulating the scanned-WMS lineshape

Molecular parameters (Eqs. 4, 7)		Laser parameters (Eqs. 1, 2)	
Line center (cm^{-1})	4,957.08	Modulation depth (cm^{-1})	0.5
Line strength ($\text{cm}^{-2} \text{atm}^{-1}$)	0.024	i_1	0.199
$2\gamma_{\text{self}}$ (296 K) ($\text{cm}^{-1} \text{atm}^{-1}$)	0.196	i_2	0.0012
n_{self}	0.73	ψ_1	3.44
$2\gamma_{\text{N}_2}$ (296 K) ($\text{cm}^{-1} \text{atm}^{-1}$)	0.143	ψ_2	3.07
n_{N_2}	0.72		

Lorentzian nature of the lineshape. When collision broadening is dominant, the peak absorbance for constant mole fraction of the collision-broadened Voigt lineshape is nearly pressure independent, while the increase in line-width scales linearly with pressure. The 1f-normalized WMS-2f lineshape is shown in Fig. 1b. One of the interesting changes observed in the 12 atm, 2f spectra is the transformation of a 3-lobed WMS lineshape into a 2-lobed structure. The disappearance of the first lobe is due to the nature of symmetric and asymmetric terms in Eqs. 13 and 14. Plots of these asymmetric and symmetric parts of the X_{2f} component of the spectra at 5 and 12 atm are shown in Fig. 2a and b, respectively. The appearance or disappearance of the first peak in the 1f-normalized WMS-2f spectrum (Fig. 1b) is governed by the relative magnitudes and shapes of the lobes in the symmetric and the asymmetric parts of the X_{2f} signal denoted by SL_1 and ASL_1 in Fig. 2a and b. At lower pressures (say 5 atm), SL_1 is prominent and higher in magnitude than ASL_1 . But with increase in pressure, the SL_1 flattens out much faster in comparison with ASL_1 , evolving into structures comparable in

magnitude and therefore canceling each other. Hence, the absolute value of the 1f-normalized WMS-2f signal morphs into a 2-lobed structure as shown in Fig. 1b.

Modulation index, defined as $m = a/HWHM$, of around 2.2 was reported to maximize the 2f signal at lower pressures in Reid and Labrie [20] and other authors [8, 22]. The increase in pressure, which blends transitions as shown in Fig. 3 for CO_2 , changes the overall shape of the absorption feature, and thus, the WMS signal. This results in a different modulation index for maximum WMS signal; an example of which for CO_2 absorption in the 2 μm band is shown in Fig. 4. This variation is obviously dependent upon the separation of the transitions and the efficiency of the broadening collisions, which in turn depends on the molecule, band, etc. Furthermore, even with a single transition, there is a slight change in the optimum modulation index with pressure, since the magnitude of 2.2 tracks the peak of the term H_2 in Eq. 13, and the contributions from the other terms rise in importance with increase in pressure. Thus, a complete simulation is required to find the optimum modulation depth for each chemical species targeted. Furthermore, at high pressures, the narrower the feature is, the larger is its WMS signal. Narrowness of the feature often becomes a more important factor than the absolute peak absorbance magnitude, as will be noted in the next few sections in the discussion about the selection of transitions.

4 Selection of transitions

First, we consider the line selection for CO which has an absorption spectrum that behaves nearly like an isolated single transition for the pressure range less than 25 atm studied here. CO_2 is considered next as it provides an

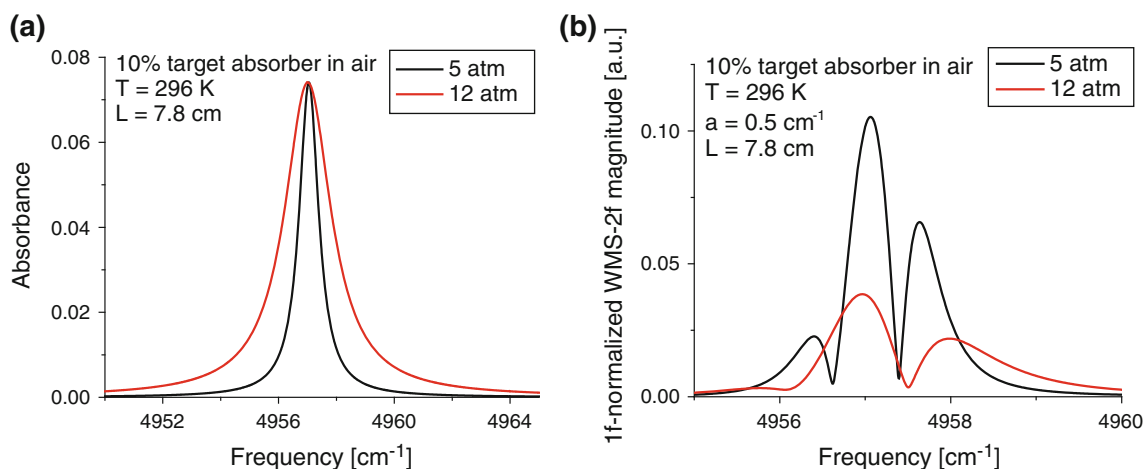


Fig. 1 a Simulated absorbance spectrum of the fictitious molecule characterized by a single transition of CO_2 near $4,957 \text{ cm}^{-1}$ at 5 and 12 atm; b 1f-normalized WMS-2f spectrum of the fictitious molecule near $4,957 \text{ cm}^{-1}$ at 5 and 12 atm

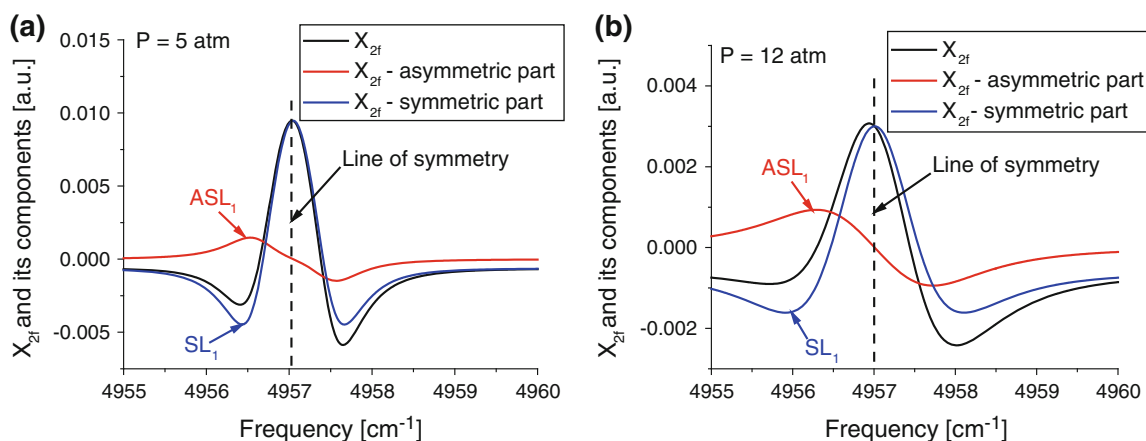


Fig. 2 WMS X_{2f} components of fictitious molecule characterized by a single transition of CO_2 near $4,957 \text{ cm}^{-1}$ at **a** 5 and **b** 12 atm

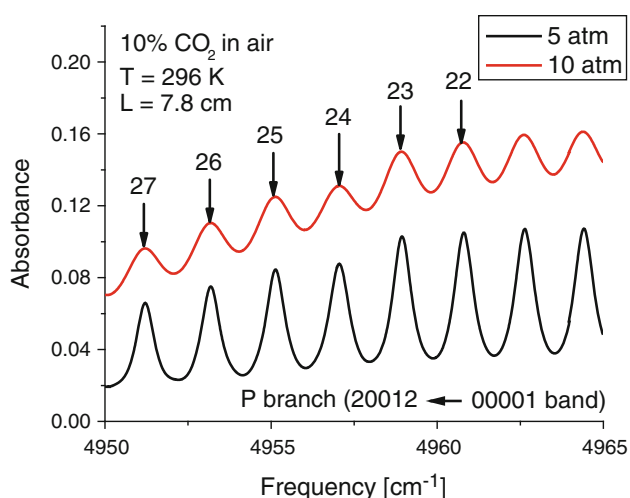


Fig. 3 Spectral lineshape blending at elevated pressures for CO_2 in the P-branch of $20012 \leftarrow 00001$ band. Numbers in the plot indicate the rotational quantum number of the lower energy state

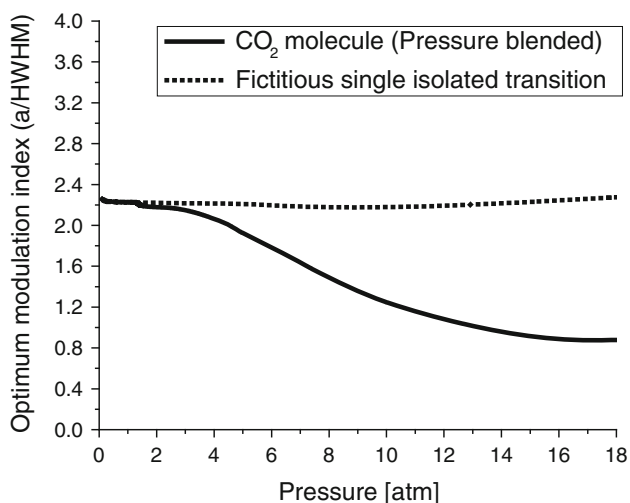


Fig. 4 Variation of the modulation index for the largest WMS-2f signal due to the blended absorbance profile of CO_2 near $4,957 \text{ cm}^{-1}$ at 296 K

example of an absorption spectrum that is severely blended at 15 atm. Finally, we consider CH_4 and H_2O , which have irregular-structured absorption spectra.

4.1 Carbon monoxide

Successful measurements of carbon monoxide were performed by Chao et al. [8] in a combustion exhaust at atmospheric pressure. The current work uses the same line (R11) in a different pressure domain. Chao et al. showed that at low concentrations of CO and high concentrations of H_2O , this line possesses the potential for a sensor with an excellent detection limit. At higher pressures, the R-branch of CO in Fig. 5 still retains its nearly resolved structure, in contrast to CO_2 , shown in Fig. 3, because the line spacing of the CO transition is about 2.3 times that of CO_2 . In this case, the sensitivity of WMS signal in the R-branch of CO at higher pressures is much less impacted by line blending. A plot of the absorbance profile of CO in the $2.3 \mu\text{m}$ band is displayed in Fig. 5a, and the WMS $2f/1f$ spectra in the vicinity of the selected transition are shown in Fig. 5b. The temperature sensitivity was calculated from the change in the absolute peak absorbance divided by the temperature change. In the 350–400 K range, this absorbance peak temperature sensitivity was $1 \times 10^{-3} \text{ K}^{-1}$ in a 30 % mixture with air. Thus, a variation of 10 K results in less than a 1 % change in the absorption signal, and this transition can provide measurements of CO that are quite insensitive to variation in gas temperature for the range studied here.

4.2 Carbon dioxide

The simulated absorbance spectra of 20 % CO_2 in air at 1 and 15 atm and 350 K, shown in Fig. 6a, reveal that the R-branch of the $2 \mu\text{m}$ absorption band of CO_2 is stronger than the P-branch. Despite this fact, the sensor transition

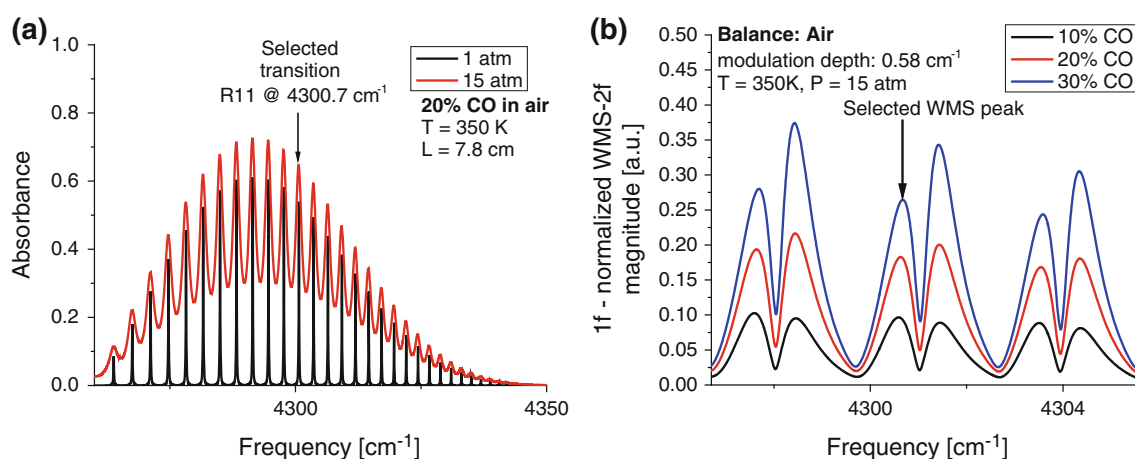


Fig. 5 **a** Absorbance spectrum of CO near $4,301\text{ cm}^{-1}$; **b** 1f-normalized WMS-2f spectrum of water near $4,301\text{ cm}^{-1}$

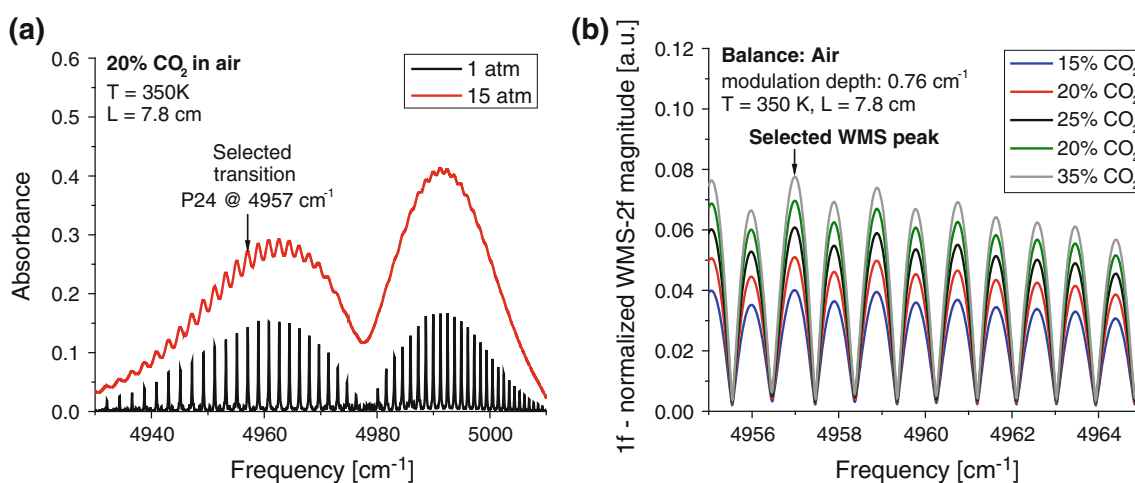


Fig. 6 **a** Absorbance spectrum of CO_2 near $4,957\text{ cm}^{-1}$; **b** 1f-normalized WMS-2f spectrum of CO_2 near $4,957\text{ cm}^{-1}$

was selected from the P-branch, since collision broadening leads to the blending of all distinct features in the R-branch at pressures as low as 15 atm (at 300 K). The line spacing in the P-branch is larger than that of the R-branch, and as a result, there are a few distinct features observable at 15 atm that can be utilized for measurements. Figure 6b displays the WMS spectra near the selected transition. This transition is primarily chosen to maximize the WMS signal. Additionally, at the gasifier temperatures of interest (300–450 K), spectral interferences from the other species are negligible. The low temperature sensitivity ($4 \times 10^{-4}\text{ K}^{-1}$ in a 30 % mixture with air) of the selected line avoids unnecessary variation of the absorption signal with mixture temperature.

4.3 Methane

Due to a generally low methane concentration in syngas, special attention was paid to the strength of the selected

transition. From Fig. 7a, it can be seen that the selected transition is the strongest and the sharpest feature in its vicinity. This has led to a larger WMS-2f/1f magnitude in comparison with its neighbors (Fig. 7b). Another important limiting aspect of this selection was presence of spectral interference from other species in the $2.25\text{ }\mu\text{m}$ band (Fig. 8). Stronger CH_4 absorption features are present in the same band at frequencies lower than $4,350\text{ cm}^{-1}$. But due to the presence of the extremely strong absorption band of CO, shown in Fig. 8, these stronger CH_4 transitions were not suitable for CH_4 sensing in syngas mixtures. Another major interfering species in this region is NH_3 . The peak absorbance of CH_4 near $4,367\text{ cm}^{-1}$ is about 14 times that of NH_3 as shown in Fig. 8. Therefore, interference from NH_3 was also minimized by the transition selection. In addition, the low temperature sensitivity of the selected transition ($2 \times 10^{-4}\text{ K}^{-1}$ for 1 % CH_4 in air) minimized the variation of the absorption signal with temperature in the range 350–400 K.

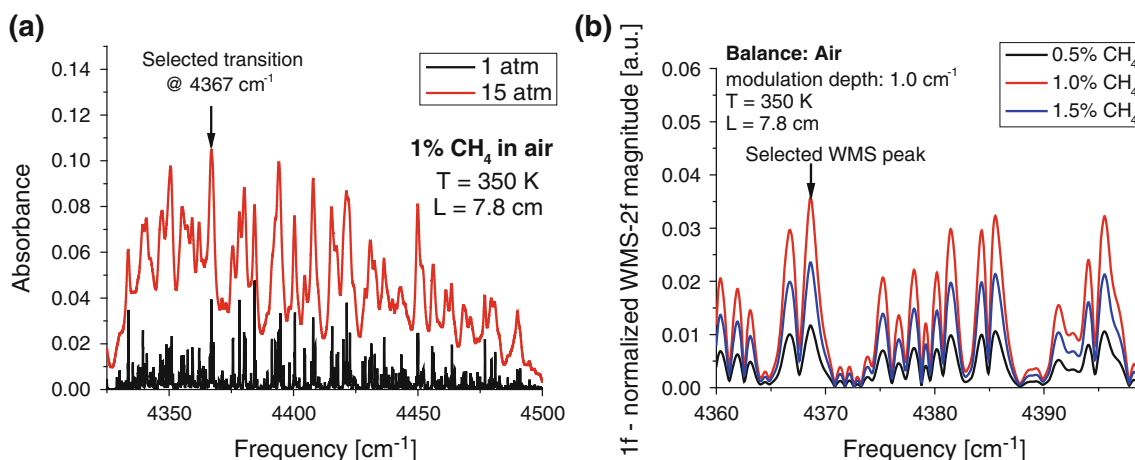


Fig. 7 **a** Absorbance spectrum of CH_4 near $4,367 \text{ cm}^{-1}$; **b** $1f$ -normalized WMS- $2f$ spectrum of CH_4 near $4,367 \text{ cm}^{-1}$

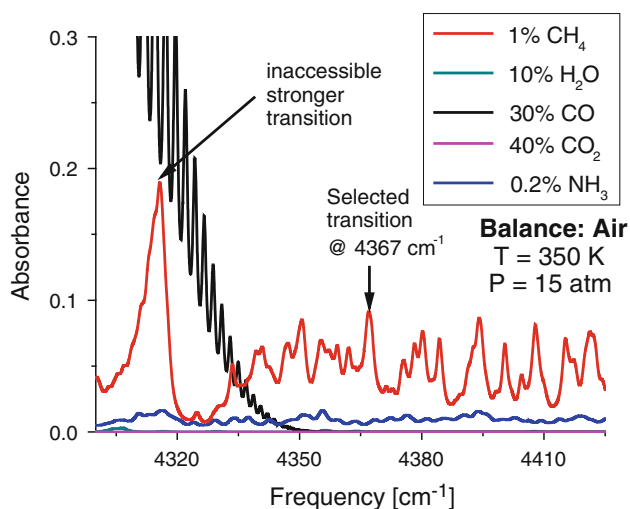


Fig. 8 Absorbance spectrum of CH_4 near $4,367 \text{ cm}^{-1}$ showing the presence of interfering species near the CH_4 absorption band used

4.4 Water

Simulations of absorbance spectra based on the HITRAN database [25] for 10 % H_2O in air near $7,400 \text{ cm}^{-1}$ at 400 K and pressures of 1 and 15 atm in air are shown in Fig. 9a. The simulations clearly show that at elevated pressures, the transitions distinctly resolved at lower pressures become blended into a few continuous features. However, the water transition near $7,394 \text{ cm}^{-1}$ has some distinctly noticeable features that led to its selection. In particular, this transition is much narrower and more isolated than the surrounding transitions. The $1f$ -normalized WMS- $2f$ spectrum for water in the vicinity of the selected transition is shown in Fig. 9b. The magnitude of the WMS spectra of this peak is larger than that of the neighbors. In addition, the peak-magnitude sensitivity to mole fraction is considerably larger than that of the neighbors as well.

Finally, due to its narrow and isolated lineshape, dependence on the broadening parameters of the neighbors is also minimal. There also was no interference absorption expected from any other major syngas component in this region. Again, this selected line has minimal sensitivity to temperature in the 350–400 K range, with a peak absorbance variation of $1 \times 10^{-3} \text{ K}^{-1}$ in a 10 % mixture with air.

5 Measurement of spectral line parameters

One of the most important steps in the development of a sensor to be employed in a multi-component mixture environment is knowledge of the transition line strengths and collision-broadening parameters of the measured species as well as those for the other major species in the mixture. For the four species concerned, the broadening parameters with all the other species, assumed here to be CO, CO_2 , H_2 , H_2O and N_2 , were measured. Due to the generally low mole fraction of CH_4 in syngas, collision broadening of the other measured species broadened by CH_4 was not investigated.

The spectroscopic parameters were measured by wavelength-scanned direct absorption as a function of pressure and temperature in a static cell of length 9.9 cm for CO, CO_2 and CH_4 and another static cell of 76.2 cm for H_2O , following the method of Arroyo et al. [26]. The cell was first filled by a known quantity of pure gas and the line-shapes of the selected transitions were acquired, e.g., for CO_2 in Fig. 10a. The linewidth of the single mode diode laser ($<0.0002 \text{ cm}^{-1}$) is neglected. The best Voigt fit of the measured lineshape was used to compute the integrated absorbance, which is proportional to the line strength and absorbing-species partial pressure, as discussed above. The

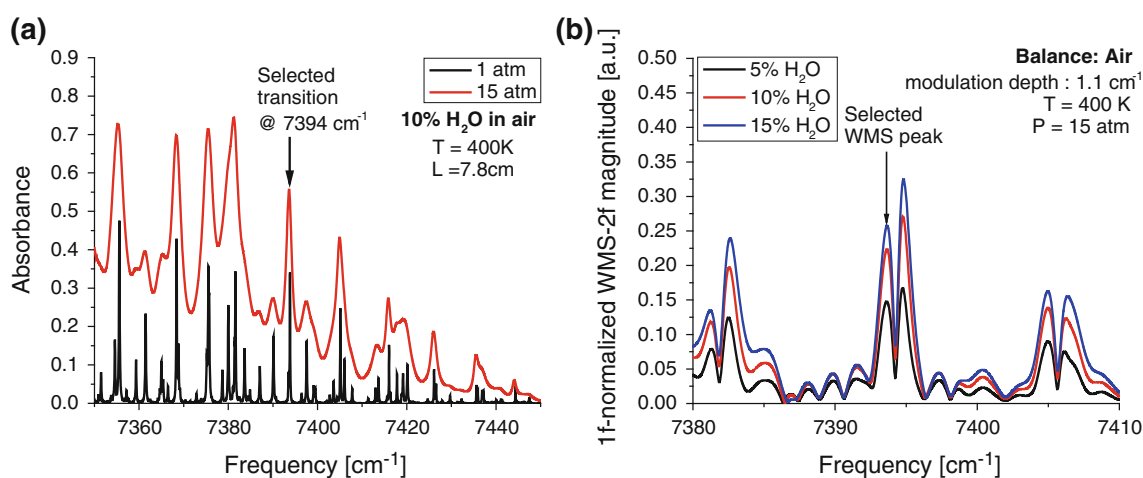


Fig. 9 **a** Absorbance spectrum of water near $7,394\text{ cm}^{-1}$; **b** 1f-normalized WMS-2f spectrum of water near $7,394\text{ cm}^{-1}$

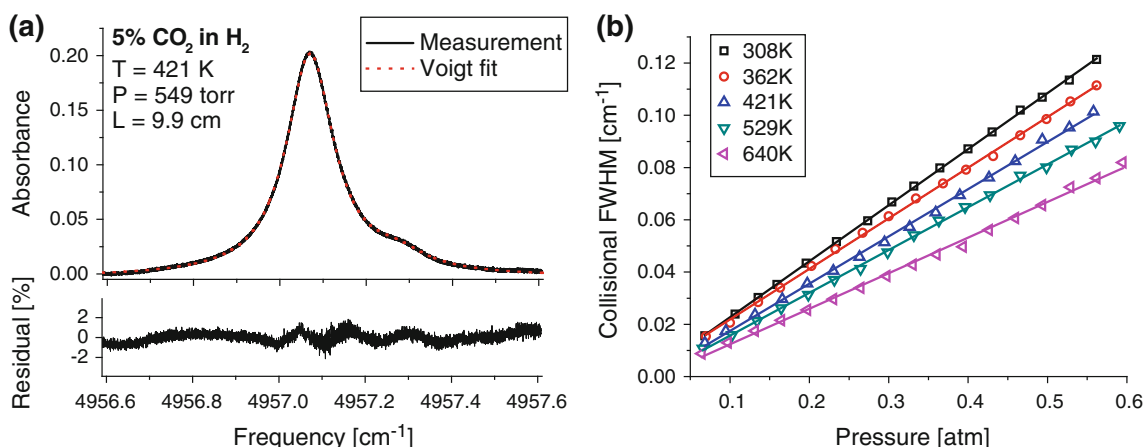


Fig. 10 **a** Sample direct absorbance spectra of CO_2 showing agreement with a Voigt fit; **b** Measured collisional FWHM for 5 % CO_2 in H_2 at different pressures

linear slope of integrated absorbance versus pressure provided the line strength.

The collision-broadening coefficients were determined from the Lorentzian-half-width parameter from Voigt fits of the lineshape with the line strength fixed. The self-broadening was first determined over a range of pressures. Then, binary mixtures of the absorbing gas with a collision partner were studied, and the absorption lineshape fit with only the width contribution of the collision partner allowed to vary. The slope of the fitted width versus pressure gives the broadening coefficient, the results of which are given in Table 2. A sample set of measurements for CO_2 broadening in H_2 is shown in Fig. 10b. The uncertainty in the measured line strengths and broadening (except water) was estimated to be within 1 and 2 %, respectively, in the measured temperature range of 300–700 K. For water broadening, this uncertainty was larger due to the reduced range of binary mixture pressures and was estimated to be less than 5 %.

6 Selection of modulation parameters

The magnitude of the 1f-normalized WMS-2f signal varies strongly with the modulation depth as discussed above. To select the optimum modulation depth for use over a range of pressures, the peak 1f-normalized WMS-2f signals were plotted versus modulation depth at different pressures. Generally, at higher pressure, the WMS signals become smaller due to the reduction in spectral curvature. Therefore, the modulation depth was optimized to enhance the higher pressure signals. As an example, Fig. 11 shows the case for the $2.0\text{ }\mu\text{m}$ laser for detection of CO_2 in a sample syngas-like mixture containing 30 % CO , 30 % CO_2 , 15 % H_2 , 15 % N_2 and 10 % H_2O . The modulation depth selected optimized the signal strength at 20 atm while retaining as much signal strength as possible at lower pressure. For CO , the optimum modulation depth could not be reached as a result of the limitation of the laser tuning

Table 2 Measured spectroscopic parameters of the selected transitions

Line center (cm^{-1})	Line strength ($\text{cm}^{-2} \text{atm}^{-1}$)	Lower state energy (cm^{-1})	$2\gamma_{\text{self}}$ [8] ($\text{cm}^{-1} \text{atm}^{-1}$)	n_{self} [8] ($\text{cm}^{-1} \text{atm}^{-1}$)	$2\gamma_{\text{N}_2}$ [8] ($\text{cm}^{-1} \text{atm}^{-1}$)	n_{N_2} [8] ($\text{cm}^{-1} \text{atm}^{-1}$)	$2\gamma_{\text{H}_2}$ ($\text{cm}^{-1} \text{atm}^{-1}$)	n_{H_2} ($\text{cm}^{-1} \text{atm}^{-1}$)	$2\gamma_{\text{CO}_2}$ [8] ($\text{cm}^{-1} \text{atm}^{-1}$)	n_{CO_2} [8] ($\text{cm}^{-1} \text{atm}^{-1}$)	$2\gamma_{\text{H}_2\text{O}}$ [8] ($\text{cm}^{-1} \text{atm}^{-1}$)	$n_{\text{H}_2\text{O}}$ [8]
<i>Carbon monoxide</i>												
4,297.70	0.0726	211.40	0.126	0.75	0.115	0.75	-	-	-	-	-	-
4,300.70	0.0649	253.67	0.124	0.71	0.114	0.70	0.147	0.55	0.144	0.69	0.252	0.96
Line center (cm^{-1})	Line strength (296 K) ($\text{cm}^{-2} \text{atm}^{-1}$)	Lower state energy (cm^{-1})	$2\gamma_{\text{self}}$ ($\text{cm}^{-1} \text{atm}^{-1}$)	n_{self} ($\text{cm}^{-1} \text{atm}^{-1}$)	$2\gamma_{\text{N}_2}$ ($\text{cm}^{-1} \text{atm}^{-1}$)	n_{N_2} ($\text{cm}^{-1} \text{atm}^{-1}$)	$2\gamma_{\text{H}_2}$ ($\text{cm}^{-1} \text{atm}^{-1}$)	n_{H_2} ($\text{cm}^{-1} \text{atm}^{-1}$)	$2\gamma_{\text{CO}}$ ($\text{cm}^{-1} \text{atm}^{-1}$)	n_{CO} ($\text{cm}^{-1} \text{atm}^{-1}$)	$2\gamma_{\text{H}_2\text{O}}$ ($\text{cm}^{-1} \text{atm}^{-1}$)	$n_{\text{H}_2\text{O}}$
<i>Carbon dioxide</i>												
4,957.08	0.02427	234.08	0.196	0.73	0.143	0.720	0.224	0.582	0.160	0.718	0.238	0.726
4,958.97	0.02648	197.41	0.200	0.68	0.145	0.700	-	-	-	-	-	-
Line center (cm^{-1})	Line strength (296 K) ($\text{cm}^{-2} \text{atm}^{-1}$)	Lower state energy (cm^{-1})	$2\gamma_{\text{self}}$ ($\text{cm}^{-1} \text{atm}^{-1}$)	n_{self} ($\text{cm}^{-1} \text{atm}^{-1}$)	$2\gamma_{\text{N}_2}$ ($\text{cm}^{-1} \text{atm}^{-1}$)	n_{N_2} ($\text{cm}^{-1} \text{atm}^{-1}$)	$2\gamma_{\text{H}_2}$ ($\text{cm}^{-1} \text{atm}^{-1}$)	n_{H_2} ($\text{cm}^{-1} \text{atm}^{-1}$)	$2\gamma_{\text{CO}_2}$ ($\text{cm}^{-1} \text{atm}^{-1}$)	n_{CO_2} ($\text{cm}^{-1} \text{atm}^{-1}$)	$2\gamma_{\text{H}_2\text{O}}$ ($\text{cm}^{-1} \text{atm}^{-1}$)	$n_{\text{H}_2\text{O}}$
<i>Methane</i>												
4,367.00	0.118	104.77	0.144	0.78	0.136	0.74	0.132	0.38	0.139	0.58	0.166	0.64
Line center (cm^{-1})	Line strength (296 K) ($\text{cm}^{-2} \text{atm}^{-1}$)	Lower state energy (cm^{-1})	$2\gamma_{\text{self}}$ ($\text{cm}^{-1} \text{atm}^{-1}$)	n_{self} ($\text{cm}^{-1} \text{atm}^{-1}$)	$2\gamma_{\text{CO}}$ ($\text{cm}^{-1} \text{atm}^{-1}$)	n_{CO} ($\text{cm}^{-1} \text{atm}^{-1}$)	$2\gamma_{\text{CO}_2}$ ($\text{cm}^{-1} \text{atm}^{-1}$)	n_{CO_2} ($\text{cm}^{-1} \text{atm}^{-1}$)	$2\gamma_{\text{N}_2}$ ($\text{cm}^{-1} \text{atm}^{-1}$)	n_{N_2} ($\text{cm}^{-1} \text{atm}^{-1}$)	$2\gamma_{\text{H}_2}$ ($\text{cm}^{-1} \text{atm}^{-1}$)	n_{H_2}
<i>Water</i>												
7,393.79	0.0178	744.06	0.478	0.73	0.128	0.800	0.150	0.959	0.093	0.547	0.082	0.462
7,393.85	0.0512	744.16	0.530	0.65	0.119	0.620	0.139	0.957	0.088	0.575	0.082	0.463

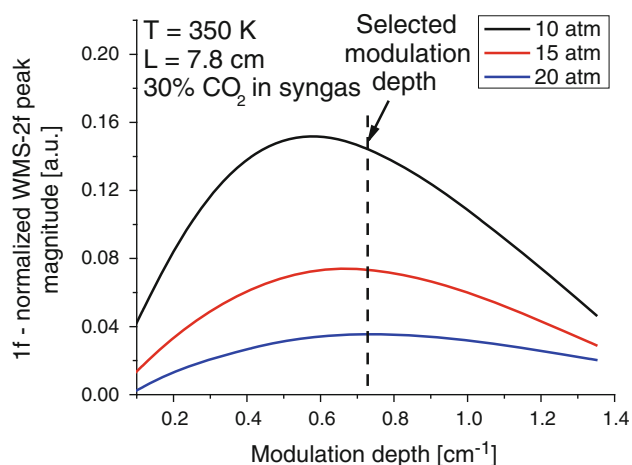


Fig. 11 Variation of 1f-normalized WMS-2f magnitude at the selected peak wavelength with modulation depth at 10 kHz modulation frequency for the laser operating at 2,017 nm for CO₂ detection at different pressures

Table 3 Selected modulation depth for the sensors

Species	Selected modulation depth (cm ⁻¹)
CO	0.58
CO ₂	0.76
CH ₄	1.02
H ₂ O	1.08

characteristics. The selected modulation depths for these sensors are listed in Table 3.

7 Sample WMS measurements of species in N₂ at elevated pressure

The first validation experiments of the sensor measured the high-pressure 1f-normalized WMS-2f spectra for a binary mixture (in this case N₂), for comparison with spectra simulated using the measured spectral database. As observed from Fig. 12, the WMS spectra at higher pressures show very good agreement with the simulations. These measurements confirm that other high-pressure phenomena that were not considered, such as line mixing and other non-Lorentzian effects, are not very important at these pressures and hence could be ignored in this work.

8 Sample WMS measurements of species in syngas mixture at different pressures

After verification of the spectra to pressures of 20 atm, the sensor was tested in different synthetic syngas mixtures of varying concentrations as a function of pressure. A

standard mixture was procured (Praxair) containing 25 % CO, 25 % H₂, 0.6 % CH₄ and balance (49.4 %) CO₂. This gas mixture was then combined with varying amounts of one of the components. Wide spectral range wavelength scans of WMS lineshape with frequency for each of the components were made with these mixtures for different pressures in a room temperature, high-pressure cell, with a path length of 23 cm. Water vapor was not included in these room temperature measurements as the vapor pressure of water is about 0.03 atm and a maximum mixture composition of 0.2 % H₂O can be produced for a mixture of 20 atm, which is much lower than the target concentration of the sensor's domain of measurement.

8.1 Carbon monoxide

The CO sensor has the advantage of largest absorbance and a well-isolated feature. This leads to a very high WMS signal level at all the pressures investigated, i.e., 5, 10, 15 and 20 atm as shown in Fig. 13a–d, respectively. The good agreement between the simulations and the measurements especially for the peak near 4,300.7 cm⁻¹ is evident from these figures.

8.2 Carbon dioxide

The CO₂ absorption spectrum is severely blended at pressures greater than 5 atm. This has a negative influence on the WMS signal strength as discussed above. Sample measured and simulated 1f-normalized WMS-2f spectra for CO₂ in a typical syngas mixture at 25 °C and at pressures of 5, 10, 15 and 20 atm are shown in Fig. 14a–d. As seen from Fig. 14d, the second lobe has completely disappeared at 20 atm. This is a result of a relatively featureless absorbance signature for CO₂ at high pressures. Despite this, the peak near 4,957 cm⁻¹ has a consistent agreement at all pressures with the simulations, thus showing suitability for CO₂ detection in syngas flows.

8.3 Methane

1f-normalized WMS-2f spectra were measured for CH₄ at a temperature of 25 °C and pressures of 5, 10, 15 and 20 atm as shown in Fig. 15a–d, respectively. In spite of having multiple lines in the region and a relatively more densely spaced spectral structure, the agreement between the simulation and the data is quite reasonable. These results serve to verify the accuracy of the mixture broadening values and the spectral modeling used.

9 Summary of the laboratory validation experiments

The gas composition of the major components of synthetic syngas determined by the sensor is compared with known

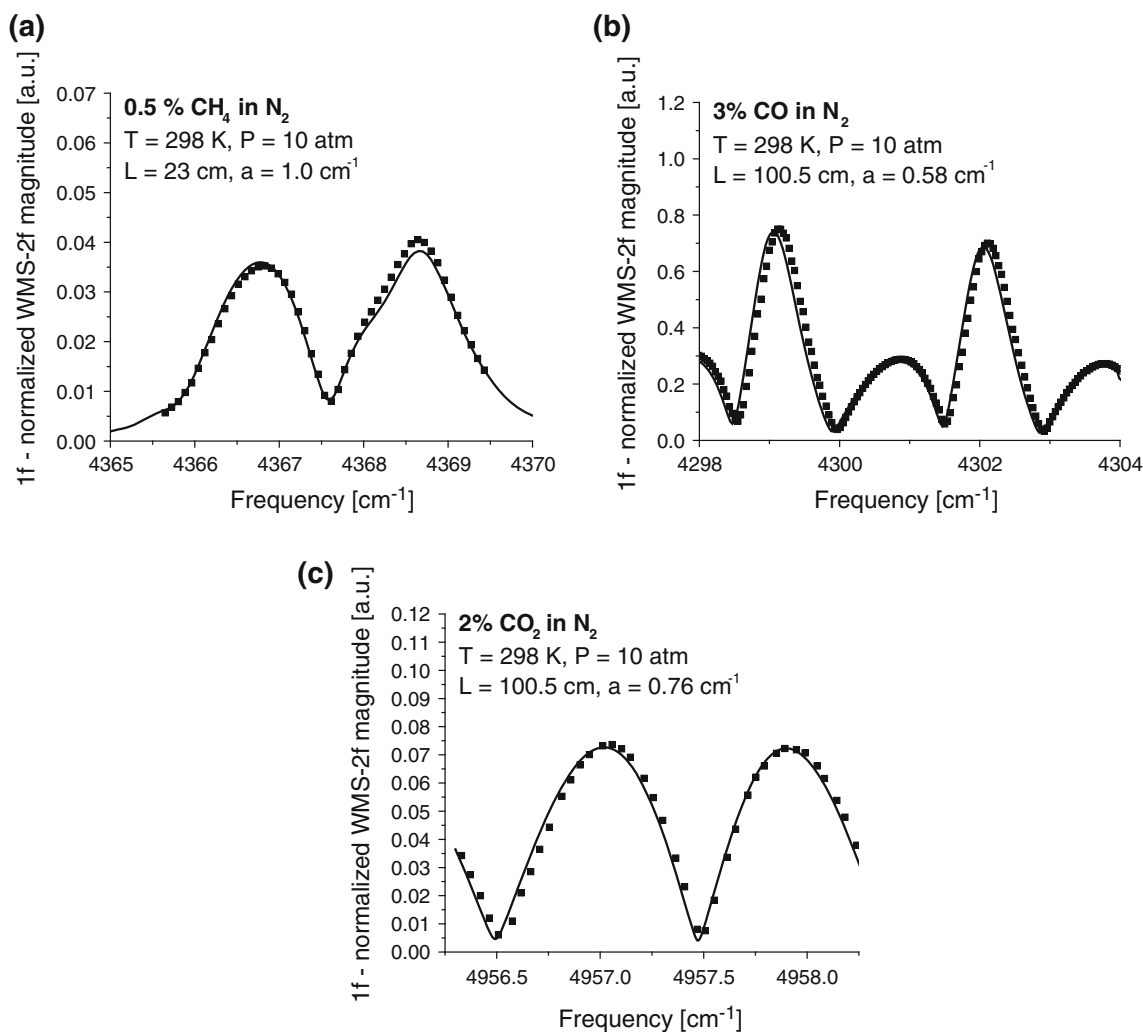


Fig. 12 Sample WMS spectra for **a** CH₄, **b** CO and **c** CO₂ in N₂ at 10 atm

values in Fig. 16. The measurements were repeated three times at the same mole fraction of CH₄ and two times for CO with different mixture compositions. These measurements consistently fell within the uncertainty of the sensor from the known value. The known mixtures were prepared by volumetric addition of varying amounts of one of the components with the base mixture of 25 % CO, 25 % H₂, 0.6 % CH₄ and balance (49.4 %) CO₂. The mixture compositions used for the validation experiments are listed in Table 4 measured data points agree with the known values within 4 %, 4 and 8 % (1, 2 and 0.05 % of total) of the measurements of the mole fraction of CO, CO₂ and CH₄, respectively. These measurements were done as a function of pressure and the general trend reflects a small increase in the difference between measured and known values with increasing pressure. The WMS signal becomes increasingly sensitive to the broadening parameters at higher pressures and these differences could be attributed to the uncertainties in the broadening coefficients. Some part of

the high-pressure differences might be also attributed to non-Lorentzian behavior of gases at higher pressures such as line mixing and finite duration of collisions.

10 Calculation of LHV and Wobbe Index of syngas mixture

The lower heating value (LHV) of a fuel is one of the most widely used properties to compare the heat release from burning different fuels. It is the amount of energy released for a specific amount of fuel through complete combustion at 25 °C and 1 atm, with the combustion products returned to the same temperature and pressure condition with saturated water vapor. When characterizing the LHV output from a gasifier, the mass basis is often chosen to be the mass of the reacted carbon present in syngas, to be indicative of the efficiency of the conversion process from the parent solid coal.

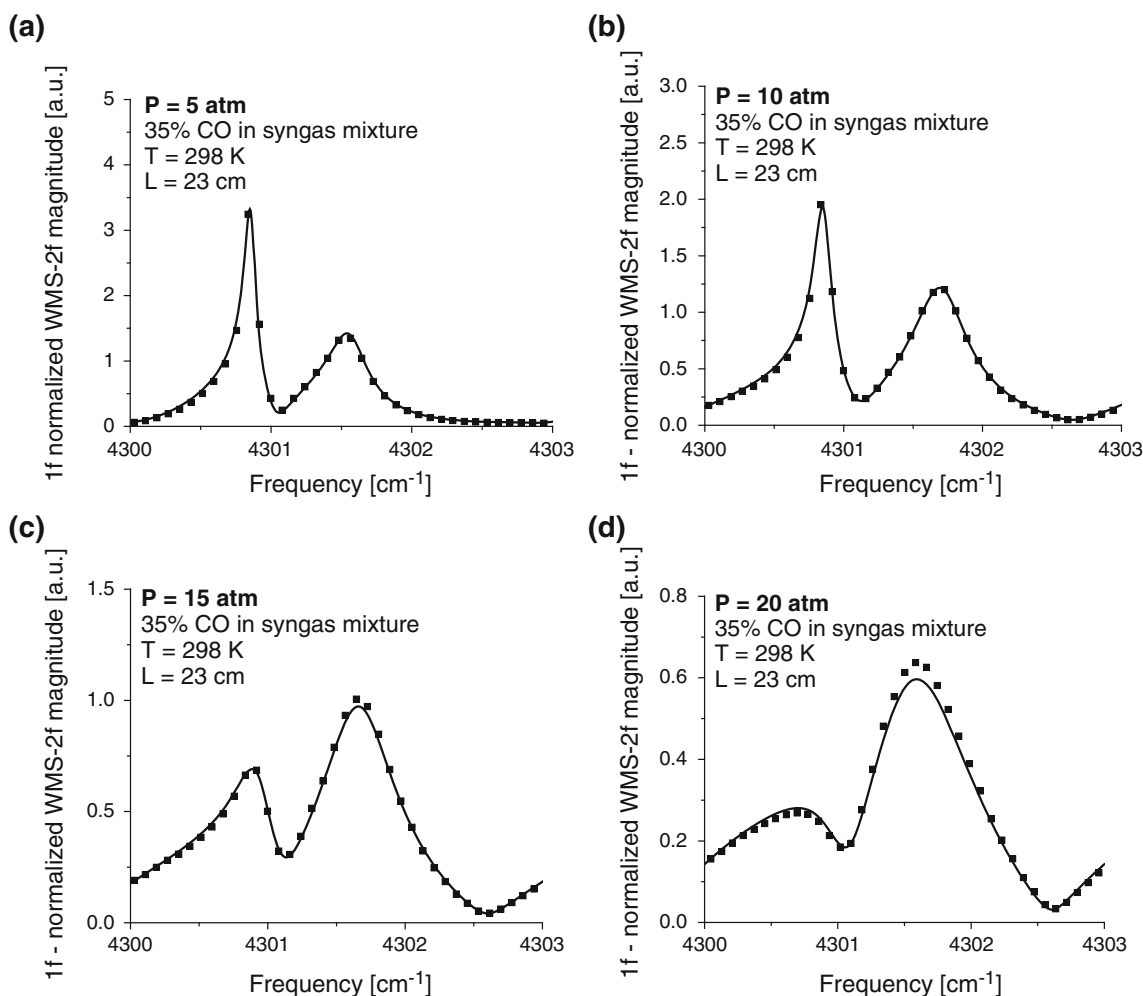


Fig. 13 Sample WMS spectra for CO in a sample syngas mixture at **a** 5 atm, **b** 10 atm, **c** 15 atm and **d** 20 atm

In general, the syngas-like mixtures are primarily composed of CO, CO₂, CH₄, H₂O and H₂ along with many trace species such as H₂S, NH₃, etc. The laser-absorption sensors described here can measure all the components except H₂, which is assumed to be the balance. This assumption provides a path to infer the lower heating value (in MJ/kg C) of the syngas as:

subscript (g) indicates the gaseous phase of water. Here, the parameters were calculated from the NIST-JANAF [27] tables, and the bimolecular species H₂ and O₂ are reference species and hence have a zero heat of formation (ΔH_f^0) at 25 °C. However, this method of obtaining the LHV is valid only for oxygen-blown gasifiers which have only low concentrations of fuel nitrogen in the syngas stream. For

$$\text{LHV} = \frac{[\Delta H_{f,\text{H}_2\text{O}(\text{g})}^0] \cdot x_{\text{H}_2} + [\Delta H_{f,\text{CO}_2}^0 - \Delta H_{f,\text{CO}}^0] \cdot x_{\text{CO}} + [2\Delta H_{f,\text{H}_2\text{O}}^0 + \Delta H_{f,\text{CO}_2}^0 - \Delta H_{f,\text{CH}_4}^0] \cdot x_{\text{CH}_4}}{M_C \cdot [x_{\text{CO}} + x_{\text{CO}_2} + x_{\text{CH}_4}]}$$

where x_i is the mole fraction, $\Delta H_{f,i}^0$ is the standard heat of formation and M_i is the molar mass of the species i . The

air-blown systems or systems with significant nitrogen purge, N₂ must also be accounted for in the syngas mixture.

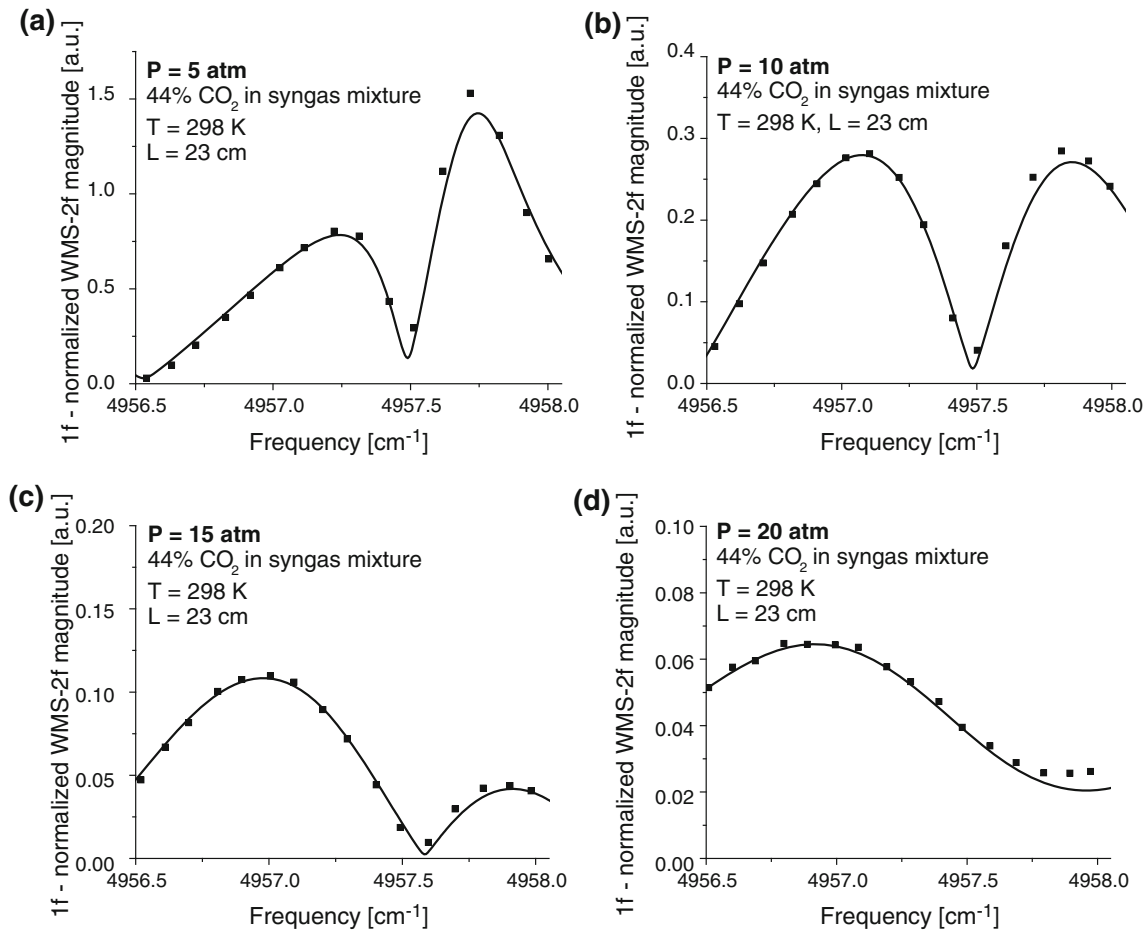


Fig. 14 Sample WMS spectra for CO₂ in a sample syngas mixture at **a** 5 atm, **b** 10 atm, **c** 15 atm and **d** 20 atm

Another parameter of importance when dealing with modern gaseous fuels is the Wobbe Index (WI), which is a measure of interchangeability of fuels. It is expressed as:

$$WI = \frac{HHV}{\sqrt{G_s}} = \frac{[\Delta H_{f,H_2O(l)}^0] \cdot x_{H_2} + [\Delta H_{f,CO_2}^0 - \Delta H_{f,CO}^0] \cdot x_{CO} + [2\Delta H_{f,H_2O}^0 + \Delta H_{f,CO_2}^0 - \Delta H_{f,CH_4}^0] \cdot x_{CH_4}}{\sqrt{G_s}}$$

where G_s is the specific gravity of the gaseous fuel with respect to dry air at 25 °C and 1 bar. The subscript (l) indicates the liquid phase of water.

The lower heating value was calculated per kilogram carbon basis for each of the syngas mixtures and compared

with the known value in Fig. 17a. A maximum scatter of less than 6 % (rms error <0.4 %) was observed for all these measurements.

Similarly, generally good agreement was achieved between the measured and the known values of the Wobbe Index as apparent from Fig. 17b. The maximum scatter observed in this case was below 8 % (rms error <0.4 %). The effective uncertainty in these inferred values from the

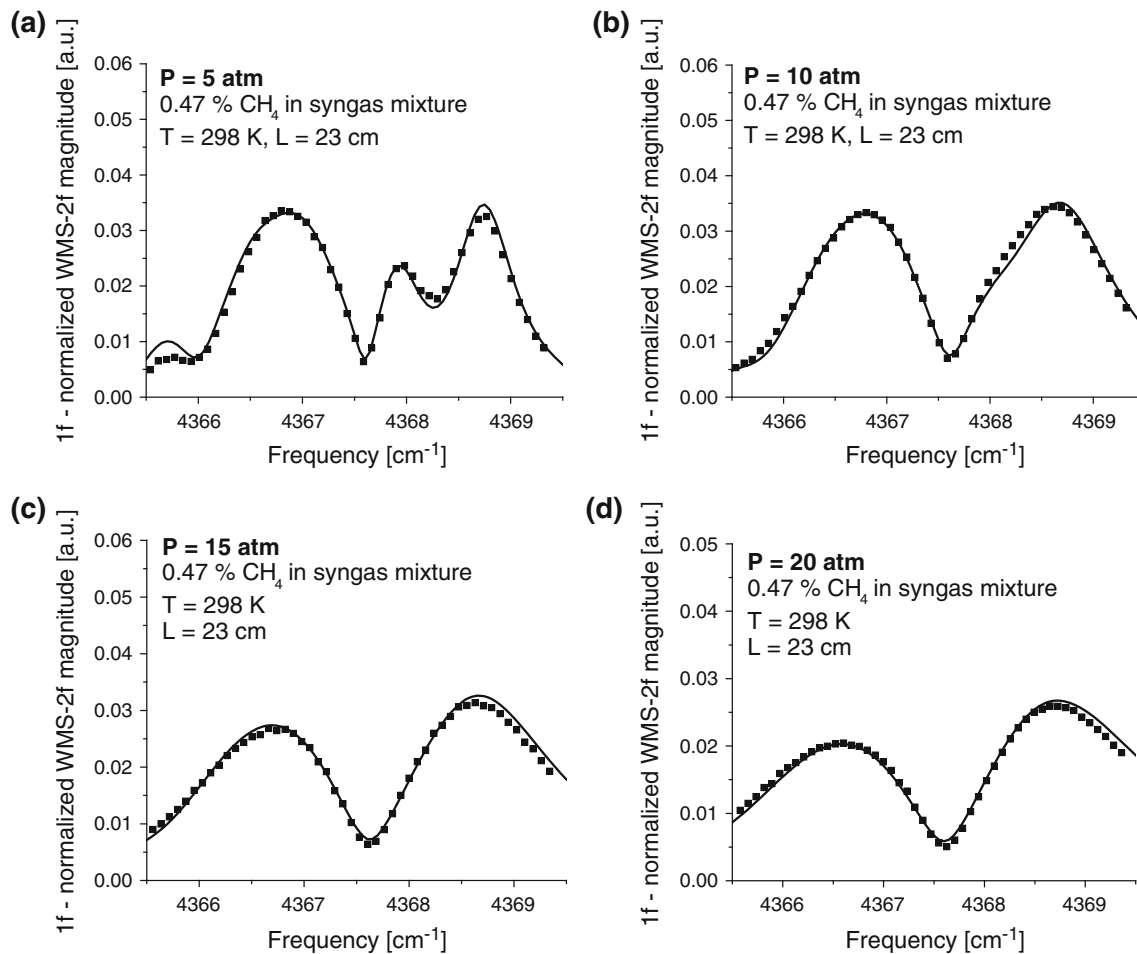


Fig. 15 Sample WMS spectra for CH_4 in a sample syngas mixture at **a** 5 atm, **b** 10 atm, **c** 15 atm and **d** 20 atm

constituents was due to the cumulative uncertainty in each of the measured components.

11 Summary

Multi-species laser absorption sensors were designed, constructed and tested to monitor the mole fraction of CO ,

CO_2 , CH_4 and H_2O in synthesis gas mixtures at pressures up to 20 atm and temperatures of 300–400 K. The sensor design was based on 1f-normalized WMS-2f detection of infrared laser absorption. The line selection was optimized for performance at high pressures and to suppress interference from typical syngas composition. A database of collision-broadening coefficients was acquired for collisions with the set of species (CO , CO_2 , H_2 , H_2O , N_2 and

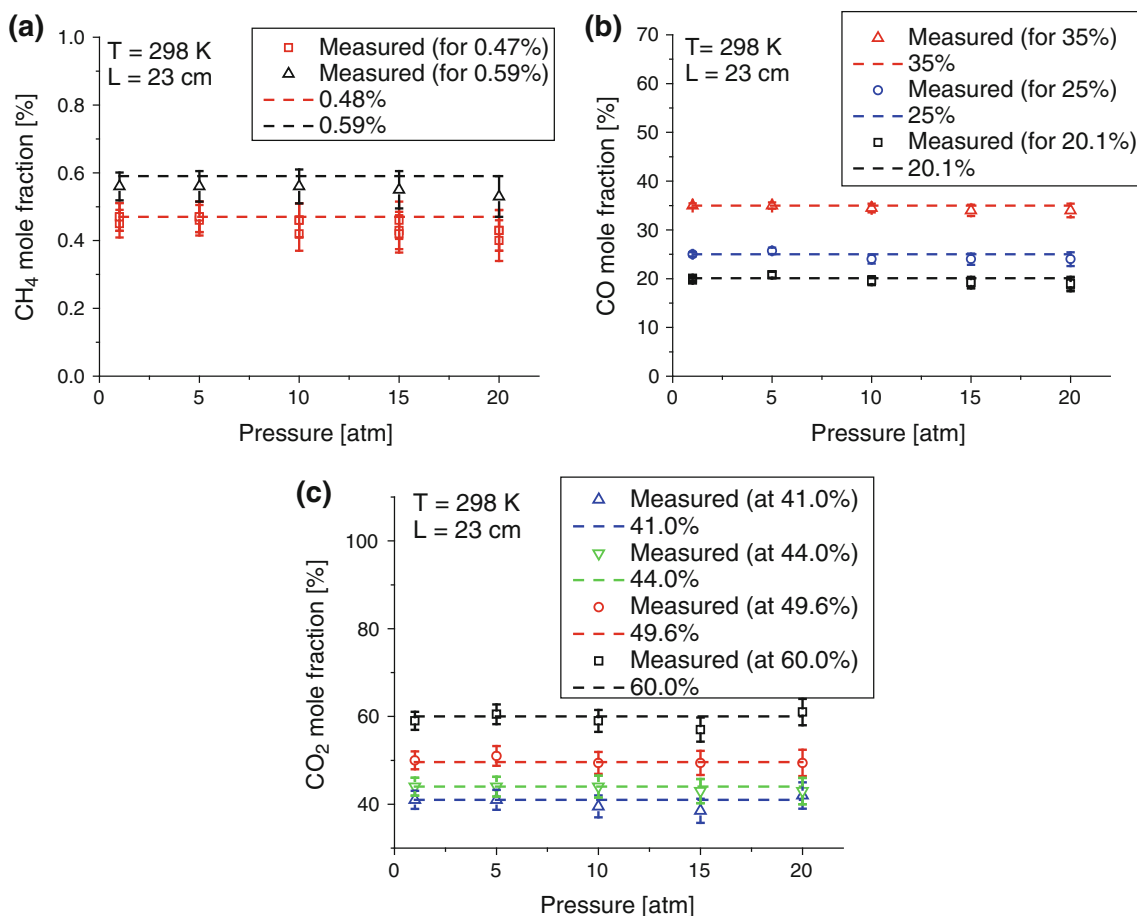


Fig. 16 Comparison between the known and the measured values of **a** CH₄, **b** CO and **c** CO₂ mol fractions in various syngas mixtures

Table 4 Percentage compositions of components in the mixtures used for the sensor validation experiments

CO	CO ₂	CH ₄	H ₂
25.0	49.6	0.6	24.8
35.0	44.0	0.5	20.5
20.1	41.0	0.5	38.4
20.1	60.0	0.5	19.4

CH₄) expected in syngas. The performance of these sensors was evaluated at room temperature up to a pressure of 20 atm. The spectral simulations for the 1f-normalized

WMS-2f signals showed agreement with the measurements in both binary mixtures with N₂ and in multi-species synthetic syngas. The lower heating value and the Wobbe index were calculated from the sensor data and compared with the known values. The inferred values were within 6 % for the LHV and 8 % for the Wobbe index over the entire pressure range. The sensor has the potential to become a reliable and fast real-time monitor for gasifier product syngas composition, with a promising future for new strategies of gasification control. The sensor was recently tested successfully in the pilot-scale entrained-flow gasifier at the University of Utah. The results of that field campaign will be published separately.

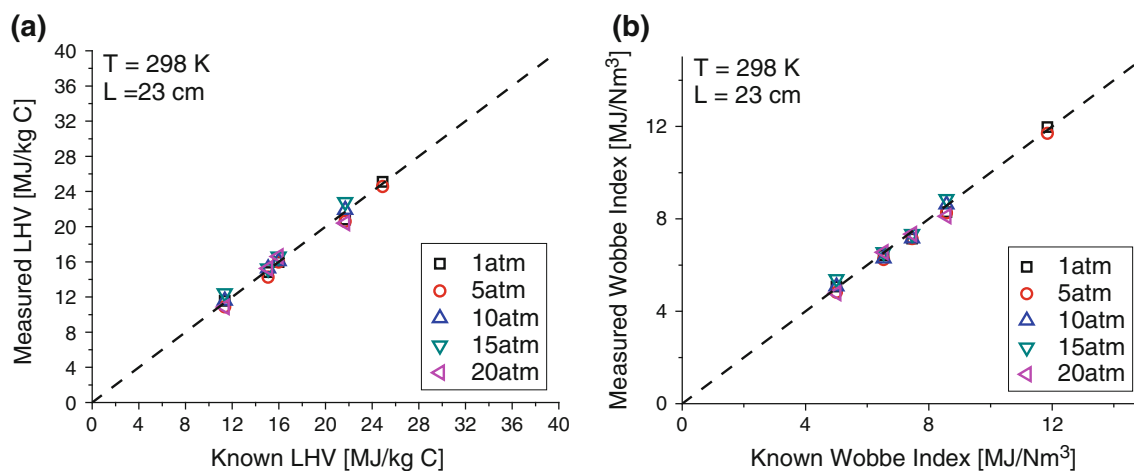


Fig. 17 Comparison between known and measured **a** LHV in MJ/kg C; **b** Wobbe index in MJ/Nm³

Acknowledgments This research was supported by the US Department of Energy (National Energy Technology Laboratory) with Dr. Susan Maley as the technical monitor and by AFOSR with Dr. Chiping Li as the technical monitor.

References

- M. Joshi, S. Lee, *Energy Sour.* **18**(5), 537 (1996)
- T.F. Wall, *Proc. Combust. Inst.* **31**, 31 (2007)
- S.J. Clayton, G.J. Stiegel, J.G. Wimer, *US DoE report DOE/FE-0447* (2002)
- R.K. Hanson, *Proc. Combust. Inst.* **33**, 1 (2011)
- P. Kluczynski, J. Gustafsson, A. Lindberg, O. Axner, *Spectrochimica Acta Part B* **56**, 1277 (2001)
- H. Teichert, T. Fernholz, V. Ebert, *Appl. Opt.* **42**, 2043 (2003)
- J. Wolfrum, *Proc. Combust. Inst.* **27**, 1 (1998)
- X. Chao, J.B. Jeffries, R.K. Hanson, *Proc. Combust. Inst.* **33**, 725 (2011)
- V. Ebert, H. Teichert, P. Strauch, T. Kolb, H. Seifert, J. Wolfrum, *Proc. Combust. Inst.* **30**, 1611 (2005)
- R.R. Skaggs, R.G. Daniel, A.W. Miziolek, K.L. McNesby, C. Herud, W.R. Bolt, D. Horton, *Appl. Spectrosc.* **53**, 1143 (1999)
- T. Gulluk, H.E. Wagner, *Rev. Sci. Instrum.* **68**, 230 (1997)
- T. Zenker, H. Fischer, C. Nikitas, U. Parchatka, G.W. Harris, D. Mihelcic, P. Musgen, H.W. Patz, M. Schultz, A. Volz-Thomas, R. Schmitt, T. Behmann, M. Weissenmayer, J.P. Burrows, *J. Geophys. Res. Atmos.* **103**, 13615 (1998)
- R. Sur, T.J. Boucher, M.R. Renfro, B.M. Cetegen, *J. Electrochem. Soc.* **157**(1), B45 (2010)
- K. Sun, R. Sur, X. Chao, J.B. Jeffries, R.K. Hanson, R.J. Pummill, K.J. Whitty, *Proc. Combust. Inst.* **34**, 3593 (2012)
- P. Ortwein, W. Woiwode, S. Fleck, M. Eberhard, T. Kolb, S. Wagner, M. Gisi, V. Ebert, *Exp. Fluids* **49**, 961 (2010)
- J.B. Jeffries, A. Fahrland, W. Min, R.K. Hanson, D. Sweeney, D. Wagner, K. J. Whitty, *Pittsburgh Coal Conference*, September (2009)
- H. Li, G.B. Rieker, X. Liu, J.B. Jeffries, R.K. Hanson, *Appl. Opt.* **45**, 1052 (2006)
- G.B. Rieker, J.B. Jeffries, R.K. Hanson, *Appl. Opt.* **48**, 5546 (2009)
- T. Fernholz, H. Teichert, V. Ebert, *Appl. Phys. B* **75**, 229 (2002)
- J. Reid, D. Labrie, *Appl. Phys. B* **26**, 203 (1981)
- R. Arndt, *J. Appl. Phys.* **36**, 2522 (1965)
- P. Kluczynski, O. Axner, *Appl. Opt.* **38**, 5803 (1999)
- K. Sun, X. Chao, R. Sur, J.B. Jeffries, R.K. Hanson, *Appl. Phys. B* **110**, 497 (2013)
- J. Humlicek, *J. Quant. Spectrosc. Radiat. Transf.* **27**(4), 437 (1982)
- L.S. Rothman et al., *J. Quant. Spectrosc. Radiat. Transf.* **110**, 533 (2009). The HITRAN database, available at <http://cfa-www.harvard.edu/hitran/>
- M.P. Arroyo, R.K. Hanson, *Appl. Opt.* **32**(30), 6104 (1993)
- M.W. Chase Jr., *JANAF-NIST thermochemical tables. J. Phys. Chem. Ref. data: Monograph No. 9* (1998)